Role of magnetic ions in the thermal Hall effect of the paramagnetic insulator TmVO$_4$

Ashvini Vallipuram [1,*,†] Lu Chen [1,*,‡] Emma Campillo [1] Manel Mezidi [1,2] Gaël Grissonnanche [3]
Marie-Eve Boulanger [1] Étienne Lefrançois [1] Mark P. Zic [4] Yuntian Li [5] Ian R. Fisher [5]
Jordan Baglo [1] and Louis Taillefer [1,6,§]

[1]*Institut quantique, Département de physique & RQMP, Université de Sherbrooke, Sherbrooke, Québec, Canada J1K 2R1*
[2]*Université Paris-Cité, Laboratoire Matériaux et Phénomènes Quantiques, CNRS (UMR 7162), 75013 Paris, France*
[3]*Laboratoire des Solides Irradiés, CEA/DRF/lRAMIS, CNRS, École Polytechnique, Institut Polytechnique de Paris, F-91128 Palaiseau, France*
[4]*Geballe Laboratory for Advanced Materials and Department of Physics, Stanford University, California 94305, USA*
[5]*Geballe Laboratory for Advanced Materials and Department of Applied Physics, Stanford University, California 94305, USA*
[6]*Canadian Institute for Advanced Research, Toronto, Ontario, Canada M5G 1M1*

In a growing number of materials, phonons have been found to generate a thermal Hall effect, but the underlying mechanism remains unclear. Inspired by previous studies that revealed the importance of Tm^{3+} ions in generating the thermal Hall effect in a family of pyrochlores, we investigated the role of Tm^{3+} ions in TmVO$_4$, a paramagnetic insulator with a different crystal structure. We observe a negative thermal Hall conductivity in TmVO$_4$ with a magnitude such that the Hall angle, $|\kappa_{xy}/\kappa_{xx}|$, is approximately 1×10^{-3} at $H = 15$ T and $T = 20$ K, typical for a phonon-generated thermal Hall effect. In contrast to the negligible κ_{xy} found in the nonmagnetic pyrochlore analog (where the Tb^{3+} ions are replaced with Y^{3+}), we observe a negative κ_{xy} in YVO$_4$ with a Hall angle of magnitude comparable to that of TmVO$_4$. This shows that the Tm^{3+} ions are not essential for the thermal Hall effect in this family of materials. Interestingly, at an intermediate Y concentration of $x = 0.3$ in Tm$_{1-x}$Y$_x$VO$_4$, κ_{xy} was found to have a positive sign, pointing to the importance of impurities in the thermal Hall effect of phonons.

I. INTRODUCTION

In the last decade, a thermal Hall effect has been measured in a number of insulators where phonons are the main heat carriers, including multiferroics such as Fe$_2$Mo$_3$O$_8$ [1], cuprates such as La$_2$CuO$_4$ [2,3] and Nd$_2$CuO$_4$ [4], nonmagnetic SrTiO$_3$ [5], and the antiferromagnet Cu$_3$TeO$_6$ [6], see Fig. 1. In Tb$_3$Ga$_5$O$_{12}$ [7], the first insulator in which a thermal Hall signal was detected, the effect was attributed to skew scattering of phonons by superstoichiometric Tb^{3+} impurities [8].

Since then, a number of theoretical scenarios have been proposed to explain the origin of the phonon thermal Hall effect. Some attribute the thermal Hall conductivity κ_{xy} to the Berry curvature of phonon bands [9]. Others link it to various types of spin-lattice coupling [10–13]. In yet others, the role of impurities is considered important [14–17], but it remains unclear which of these scenarios applies to what material.

In a previous study on pyrochlores [18], a sizable κ_{xy} was observed in Tb$_2$Ti$_2$O$_7$ but a negligible κ_{xy} was detected in Y$_2$Ti$_2$O$_7$. Although the κ_{xy} signal in Tb$_2$Ti$_2$O$_7$ was originally attributed to some exotic neutral excitations linked to the spin-liquid nature of the system [18], it was later argued that phonons are, in fact, responsible for the thermal Hall effect in

this material [19] since a κ_{xy} signal of comparable magnitude is still observed when 70% of the Tb^{3+} ions are replaced by Y^{3+} ions, and the spin state of the system is profoundly altered. Irrespective of the underlying mechanism, this study does show that Tb^{3+} ions are essential for generating a thermal Hall effect in these pyrochlores.

Here we report a similar study carried out on a different oxide, TmVO$_4$, wherein we investigate what happens to the thermal Hall effect when we substitute the magnetic ion Tm^{3+} for the nonmagnetic ion Y^{3+}.

The insulator TmVO$_4$ exhibits a rich set of phenomena at low temperatures. It undergoes a cooperative Jahn-Teller phase transition at $T = T_D \simeq 2$ K in zero field and at $H = H_D \simeq 0.5$ T at $T = 0$ (for $H//c$) [25]. (Note that we use H as a shorthand notation for $\mu_0 H$.) The ordered state consists of a simultaneous ferroquadrupole order of the local $4f$ electronic orbitals of each Tm atom, accompanied by a structural transition, by which the crystal structure goes from tetragonal at high temperature ($I41/amd$ space group [21]) to orthorhombic at low temperature [25–29]. However, no magnetically ordered state has been reported in TmVO$_4$ [25]. Our own study will focus on temperatures above T_D.

II. METHODS

A. Samples

The following three rare-earth vanadates were studied: TmVO$_4$, YVO$_4$, and Tm$_{0.7}$Y$_{0.3}$VO$_4$. The samples were grown using a flux growth method [30,31]. They are needle-shaped
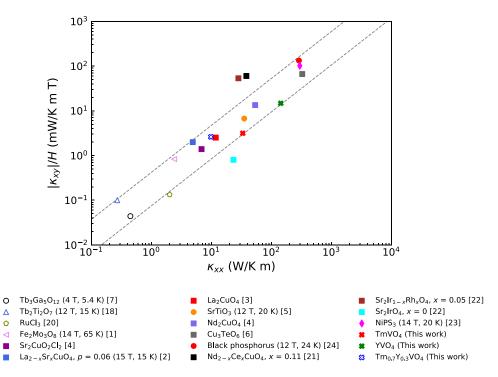

045144-1

FIG. 1. Phonon thermal Hall conductivity normalized by field $|\kappa_{xy}|/H$ of various insulators [1,3–7,19–23] as a function of their thermal conductivity, κ_{xx}. The data are taken at $H = 15$ T and $T = 20$ K unless indicated otherwise. This figure is inspired by a similar plot from Li *et al.* [24], to which other data points have been added, including those from our three samples. The gray lines mark the region where most values of κ_{xy} are found, showing that κ_{xy} scales with κ_{xx}, as emphasized previously [1,4,6,24]. The data points that lie outside the delineated region are $Nd_{2-x}Ce_xCuO_4$ at $x = 0.11$ [21] and $Sr_2Ir_{1-x}Rh_xO_4$ at $x = 0$ as well as $x = 0.05$ [22] (see text). Open (full) symbols indicate a positive (negative) κ_{xy}.

with their long axis along the c axis, which is the easy axis of magnetization [32]. Because $TmVO_4$ has a large anisotropy in its g-factor ($g_c = 10$ and $g_a = g_b = 0$) [33], even a slight misalignment of the magnetic field can cause a large torque on the sample, which can detach it from its mount.

Two measures were adopted to prevent this. First, the thermal transport contacts on $TmVO_4$ and $Tm_{0.7}Y_{0.3}VO_4$ samples were made with silver epoxy to ensure strong contacts that would adhere to a very smooth surface and would not peel off. These contacts were solidified for about 10 minutes on a hot plate at $150°$ C. Note that the contacts on the YVO_4 samples were done with silver paint since there is no magnetic torque in this case. For the heater contact, a 50-μm diameter silver wire was used and for the thermal transport contacts, wires with a diameter of 25 μm were used.

In addition, a small wood stick was positioned along the $TmVO_4$ and $Tm_{0.7}Y_{0.3}VO_4$ samples, and was linked to the sample by the heater wire. The thermal conductivity κ_{xx} was measured (in zero field) with and without the wood stick and only a 5% (8%) difference was observed at the peak temperature for $TmVO_4$ ($Tm_{0.7}Y_{0.3}VO_4$). The sample dimensions (contact dimensions) are given in Table I.

B. Thermal transport measurements

To perform a conventional thermal transport study, a five-contact measurement is done using a steady-state method at a fixed field, as sketched in Fig. 2. A heat current ($\vec{J}$) is

generated along the x axis from the heater contact on one end of the sample and the copper block on the other end. The heater is a strain gauge of 5 kΩ whose resistance does not change with temperature or field. (No potential strain is conferred to the sample since the heater is glued with GE varnish to a silver pad.) This heat current was applied along the c axis of the sample (the x axis in Fig. 2), while the field H was applied along the a axis (the z axis in Fig. 2). Note that the field ($H = 10$ or 15 T) was applied at high temperatures (at 83 K) and the samples were cooled down to $\simeq 3$ K using a variable temperature insert (VTI). This procedure ensures that no hysteresis due to the sample is generated.

Temperature steps from $\simeq 3$ K to 80 K were done at fixed fields and all the temperature signals were stable before measuring each temperature difference (ΔT_x and ΔT_y in Fig. 2) using type-E (chromium/constantan) thermocouples. Note that a test has been done previously to show that thermocouples and chip-based thermometers (Cernox) yield the same thermal Hall data (see Appendix C in Ref. [34]). Also,

TABLE I. Dimensions of the three samples investigated here. $L =$ length between contacts; $w =$ width of the sample; $t =$ thickness of the sample.

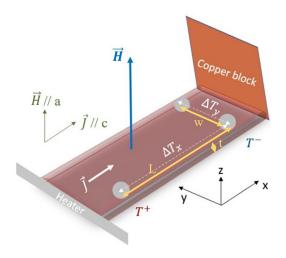|	L (mm)	w (mm)	t (mm)
$TmVO_4$	0.66	0.24	0.04
YVO_4	0.49	0.25	0.06
$Tm_{0.7}Y_{0.3}VO_4$	0.65	0.45	0.04

FIG. 2. Experimental setup used to measure κ_{xx} and κ_{xy}. A heat current J is generated along the x axis (c axis of the sample) and a magnetic field H is applied perpendicular to it, along the z axis (a axis of the sample). Differences in temperature are measured along the x axis (longitudinal temperature difference $\Delta T_x = T^+ - T^-$) and the y axis (transverse temperature difference ΔT_y).

note that for all the voltages, the background voltage (when the heat is off) is subtracted from the measured signal (when the heat is on).

The conductivities κ_{xx} and κ_{xy} were measured as described elsewhere [2–4]. Note that the transverse temperature difference ΔT_y is obtained by measuring in both field polarities ($+H$ and $-H$). We checked that our technique is independent of the particular choice of sequence, i.e., whether we measure $+H$ first and then $-H$ or if we measure instead $-H$ first and then $+H$. This means that our experimental setup and our procedure do not generate any (technique dependent) hysteresis. Then, we antisymmetrize the measured signals to get rid of any longitudinal contribution due to a possible slight misalignment of the transverse contacts

$$\Delta T_y(T, H) = [\Delta T_y(T, +H) - \Delta T_y(T, -H)]/2. \quad (1)$$

The sign of ΔT_y is determined by measuring a sample of known κ_{xy} with the same setup and wiring. In a metallic sample with Hall coefficient $R_H > 0$ (thus an electrical Hall conductivity $\sigma_{xy} > 0$), the thermal Hall conductivity κ_{xy} will be positive (at least in the $T = 0$ limit) since both thermal and electrical conductivities are related by the Wiedemann-Franz law $\kappa_{xy}/T = L_0 \sigma_{xy}$ for $T \to 0$.

The thermal conductivity is defined as

$$\kappa_{xx} = \frac{J}{\Delta T_x \, \alpha}, \quad (2)$$

where J is the heat current (in W) and α is a geometric factor ($\alpha = \frac{wt}{L}$; see Table I for sample dimensions). The thermal Hall conductivity is defined as

$$\kappa_{xy} = \kappa_{yy} \left(\frac{\Delta T_y}{\Delta T_x} \right) \left(\frac{L}{w} \right). \quad (3)$$

Note that here we assume that $\kappa_{yy} = \kappa_{xx}$ (i.e., that $\kappa_a = \kappa_c$), but this is not quite right since the c axis conductivity is not identical to the a axis conductivity. This implies that the
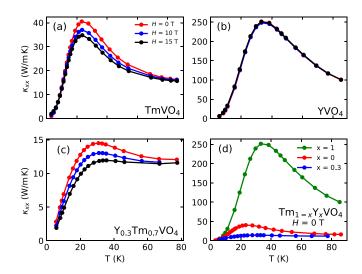

FIG. 3. Thermal conductivity of (a) TmVO$_4$, (b) YVO$_4$, and (c) Tm$_{0.7}$Y$_{0.3}$VO$_4$ as a function of temperature, measured with a heat current $J//c$ and a magnetic field $H//a$ ($H \perp J$, for $H = 0$ (red), 10 T (blue), and 15 T (black). (d) Comparison of the three conductivities at $H = 0$. We see that substituting Y for Tm causes a major reduction in κ_{xx}, which is then further reduced if Y impurities are added.

amplitude of κ_{xy} reported here is not quite accurate, and would need to be multiplied by the anisotropy factor κ_a/κ_c. Given the needle shape of our samples, measurements with $J//a$ have not been done.

III. RESULTS

A. Thermal conductivity, κ_{xx}

The thermal conductivity κ_{xx} of our three samples is displayed in Fig. 3. All three curves are typical of insulators, with a peak near $T \simeq 20$–30 K.

The thermal conductivity of TmVO$_4$ was measured previously [35]. These early measurements were done with $J//H//c$ (along the easy axis [32]) for $H < 7$ T and for $T < 30$ K, whereas our measurements were done with $J//c$ and $H//a$, covering a larger temperature and field range. This previous study reports a slightly higher κ_{xx} peak, perhaps due to larger samples and higher sample quality. The field was found to increase κ_{xx} at low temperatures ($T < 6$ K). In our study, we also see an increase in κ_{xx} with H at low temperatures [$T < 10$ K; inset of Fig. 4(a)].

The zero-field curves are compared in Fig. 3(d), where we see that κ_{xx} in YVO$_4$ is much larger than in the other two samples. The magnitude of κ_{xx} in the stoichiometric sample of paramagnetic TmVO$_4$ is much lower presumably because phonons scatter on the crystal field levels of the Tm^{3+} ions. This is also presumed to be the case in the frustrated spin system Tb$_2$Ti$_2$O$_7$, where the scattering of phonons would involve the crystal field levels of the Tb^{3+} ions, as argued previously [8]. This scattering process is much stronger for Tb^{3+} than Tm^{3+}, resulting in a value of $\kappa_{xx} \simeq 2$ W/m K at $T = 20$ K in Tb$_2$Ti$_2$O$_7$ [36], compared to $\kappa_{xx} \simeq 40$ W/m K in TmVO$_4$ [Fig. 3(a)].

As in the case of Tb$_2$Ti$_2$O$_7$, where the field dependence of κ_{xx} is exceptionally strong [36], we view the sizable field
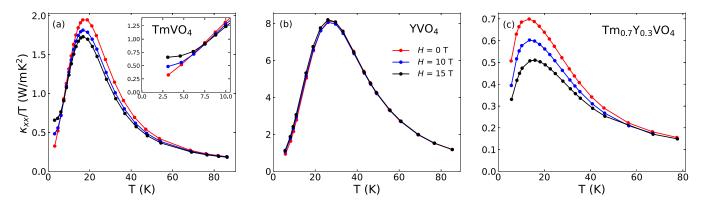
FIG. 4. Thermal conductivity of (a) TmVO$_4$, (b) YVO$_4$, and (c) Tm$_{0.7}$Y$_{0.3}$VO$_4$, for different applied magnetic fields, as indicated, plotted as κ_{xx}/T versus T to emphasize the low-temperature regime. Note the strong field dependence in the two samples that contain Tm^{3+} ions, compared to the much weaker field dependence in YVO$_4$. In panel (a), the inset shows a zoom below 10 K, where we see a different regime of H dependence, with a strong increase in κ_{xx} with increasing H.

dependence of κ_{xx} in TmVO$_4$ [Fig. 3(a)] and Tm$_{0.7}$Y$_{0.3}$VO$_4$ [Fig. 3(c)], as a confirmation that phonons are scattered by the crystal field levels of the Tm^{3+} ions. The weaker field dependence seen in YVO$_4$ [Fig. 3(b)] is consistent with that picture. We attribute the fact that κ_{xx} in Tm$_{0.7}$Y$_{0.3}$VO$_4$ is even smaller than in TmVO$_4$ to the extra disorder introduced by the Y impurities [Fig. 3(d)].

In Fig. 4, we plot κ_{xx}/T versus T to emphasize the data at low temperature. We see that below ~ 10 K or so, the field dependence of κ_{xx} in TmVO$_4$ becomes very strong and opposite in sign relative to its behavior at higher temperature [inset of Fig. 4(a)]. We speculate that this change of behavior is associated with the quadratic splitting of the crystal field levels of the Tm^{3+} ions with field (second-order Zeeman interaction for $H//a$) [25] which changes the resonant phonon scattering (for phonons of appropriate symmetry).

Interestingly, this change in field dependence, as the temperature is raised, was actually captured by theoretical calculations that consider the main scattering mechanism of phonons to be resonant scattering on electronic levels of the Tm^{3+} ions [37,38], albeit for temperatures much closer to the transition.

B. Thermal Hall conductivity, κ_{xy}

The thermal Hall conductivity κ_{xy} of our three samples is displayed in Fig. 5. Only data at $H = 15$ T are shown, but data at $H = 10$ T were also taken; they are similar but smaller in magnitude, roughly in proportion to the field amplitude. The first observation is that all three samples exhibit a non-negligible thermal Hall conductivity. The surprise is that the sign of κ_{xy} is negative in the two stoichiometric materials, TmVO$_4$ and YVO$_4$, but it is positive in the disordered sample Tm$_{0.7}$Y$_{0.3}$VO$_4$.

We see that the temperature at which $\kappa_{xy}(T)$ peaks (Fig. 5) is roughly the same as the temperature at which the phonon-dominated $\kappa_{xx}(T)$ peaks (Fig. 3), for example, $\simeq 25$ K in TmVO$_4$ and $\simeq 35$ K in YVO$_4$. As argued before for other materials [4–6,24], this is an argument in support of phonons being the heat carriers responsible for the thermal Hall signal in these materials.

Looking at Fig. 5, we also notice that the magnitude of κ_{xy} appears to roughly scale with the magnitude of κ_{xx} seen in Fig. 3(d). This is confirmed when looking at the thermal Hall angle, plotted as $|\kappa_{xy}/\kappa_{xx}|$ versus T in Fig. 6. Indeed, we see that $|\kappa_{xy}/\kappa_{xx}| \simeq 1 \times 10^{-3}$ at $T \sim 20$ K in both YVO$_4$ and Tm$_{0.7}$Y$_{0.3}$VO$_4$, even though the magnitude of κ_{xy} is 25 times larger in YVO$_4$ (Fig. 5). This is because κ_{xx} is also roughly 25 times larger in YVO$_4$ (Fig. 3).

IV. DISCUSSION

In the pyrochlore study, a nonzero (and positive) thermal Hall effect was measured in Tb$_2$Ti$_2$O$_7$, but a negligible κ_{xy} was detected in Y$_2$Ti$_2$O$_7$ [18]. It was initially speculated that the thermal Hall signal in Tb$_2$Ti$_2$O$_7$ was due to some exotic spin excitations [18]. However, a subsequent study found that the κ_{xy} signal remains as strong when 70% of the magnetic Tb^{3+} ions are replaced by nonmagnetic Y^{3+} ions, thereby dramatically altering the frustrated spin-liquid state of pure
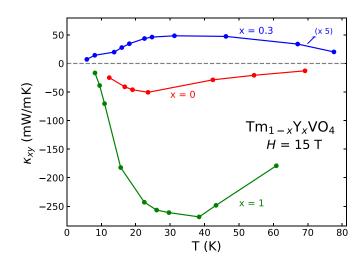

FIG. 5. Thermal Hall conductivity of TmVO$_4$ (red), YVO$_4$ (green), and Tm$_{0.7}$Y$_{0.3}$VO$_4$ (blue) as a function of temperature, measured with a heat current $J//c$ and a magnetic field $H//a$ ($H \perp J$), at $H = 15$ T. Note that κ_{xy} for Tm$_{0.7}$Y$_{0.3}$VO$_4$ has been multiplied by a factor of 5.
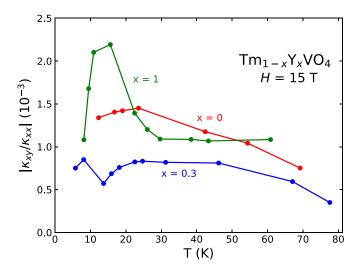
FIG. 6. Thermal Hall angle of TmVO$_4$ (red), YVO$_4$ (green), and Tm$_{0.7}$Y$_{0.3}$VO$_4$ (blue), plotted as $|\kappa_{xy}/\kappa_{xx}|$ versus T, for $H = 15$ T. At $T = 20$ K, the obtained value is around 1×10^{-3} for all three materials, a magnitude typical of the phonon Hall effect in several insulators [6,24] (see Fig. 1).

Tb$_2$Ti$_2$O$_7$ [19]. This lead to the conclusion that phonons are, in fact, the heat carriers responsible for the thermal Hall effect in these pyrochlores. Moreover, the fact that κ_{xy} becomes negligible in Y$_2$Ti$_2$O$_7$, when all Tb is replaced by Y, suggests that magnetism plays a key role in the generation of the phonon thermal Hall effect in these pyrochlores.

Turning to our own study, we also observe a nonzero κ_{xy} in TmVO$_4$, another oxide with magnetic ions (Tm^{3+}), and we also attribute this Hall effect to phonons, as argued above. In our comparison with Tb$_2$Ti$_2$O$_7$, we see two differences. The first is the fact that our nonmagnetic parent compound, YVO$_4$, also displays a nonzero κ_{xy}, unlike the negligible signal of Y$_2$Ti$_2$O$_7$. So in these vanadates, the phonon Hall effect does not depend crucially on the magnetic moment associated with Tm^{3+} ions. Note that a nonzero thermal Hall effect from phonons has been observed in other nonmagnetic insulators, such as strontium titanate [5] and black phosphorous [24].

The second difference is the sign of κ_{xy}: positive in Tb$_2$Ti$_2$O$_7$, negative in TmVO$_4$. The sign of the phonon Hall conductivity is an entirely open question, on which existing theories shed little light. Phenomenologically, both signs are observed, see Fig. 1. For example, the phononic κ_{xy} is negative in SrTiO$_3$ [5], Cu$_3$TeO$_6$ [6], and black phosphorus [24], as well as in all cuprates, whether undoped [3,4], hole-doped [2], or electron-doped [21]. A positive phononic κ_{xy} is observed in Fe$_2$Mo$_3$O$_8$ [1], (Tb$_{0.3}$Y$_{0.7}$)$_2$Ti$_2$O$_7$ [19], and RuCl$_3$ [20,39]. A remarkable feature of our findings is that κ_{xy} changes sign to positive upon introducing 30% Y into TmVO$_4$ (Fig. 5). This suggests that impurities, in much larger concentration in Tm$_{0.7}$Y$_{0.3}$VO$_4$ relative to either TmVO$_4$ or YVO$_4$, is an important ingredient for the generation of a phonon thermal Hall effect.

It is instructive to look at the magnitude of κ_{xy}. As argued by others [1,6,24], the relevant quantity for this is the ratio κ_{xy}/κ_{xx}, namely, the Hall angle. In Fig. 6, we see that in our three samples $|\kappa_{xy}/\kappa_{xx}| \simeq 1 \times 10^{-3}$ at $T = 20$ K and $H = 15$ T. This is quite typical. Indeed, the cuprate Mott

insulators La$_2$CuO$_4$, Nd$_2$CuO$_4$, and Sr$_2$CuO$_2$Cl$_2$ and the antiferromagnetic insulator Cu$_3$TeO$_6$ all have a Hall angle of about 3×10^{-3} at the same temperature and field [6]. The Kitaev spin liquid candidate RuCl$_3$ has a Hall angle of about 1×10^{-3}. Note that the magnitude of κ_{xy} varies by three orders of magnitude across those various materials (see Fig. 1).

It is worth noting that significantly larger thermal Hall angles have been observed in two cases so far: the Ce-doped cuprate Nd$_2$CuO$_4$ [21] and the Rh-doped iridate Sr$_2$IrO$_4$ [22]. In as-grown samples of Nd$_2$CuO$_4$ with 11% Ce and Sr$_2$IrO$_4$ with 5% Rh, $|\kappa_{xy}/\kappa_{xx}| \simeq 30 \times 10^{-3}$ at $T = 20$ K and $H = 15$ T. Both materials are insulators with antiferromagnetic order at these dopings, and it was argued in the latter study that impurities embedded in an antiferromagnetic environment strongly promote the phonon thermal Hall effect [22], as suggested theoretically for a mechanism of resonant side-jump scattering of phonons [17].

V. SUMMARY

We measured a nonzero thermal Hall conductivity κ_{xy} in the vanadates TmVO$_4$, YVO$_4$ and Tm$_{0.7}$Y$_{0.3}$VO$_4$. All evidence points to phonons as the heat carriers responsible for generating this Hall effect. The magnitude of the Hall response is similar in all three, with a Hall angle of $|\kappa_{xy}/\kappa_{xx}| \simeq 1 \times 10^{-3}$ at $T = 20$ K and $H = 15$ T, comparable to the phonon Hall effect in several insulating materials. This shows that Tm^{3+} ions do not play an essential role in generating the Hall effect in these rare-earth vanadates. While the sign of κ_{xy} in the two stoichiometric compounds TmVO$_4$ and YVO$_4$ is negative, we find a positive sign in the more disordered Tm$_{0.7}$Y$_{0.3}$VO$_4$. This points to a special role played by impurities in this family of materials.

APPENDIX

The thermal Hall effect can be measured in three ways and we have tested these methods on the hole-doped cuprate La$_{2-x}$Sr$_x$CuO$_4$ $p = 0.06$ (LSCO).
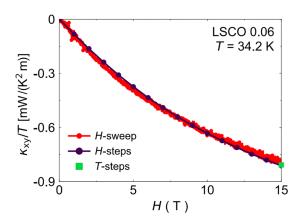
FIG. 7. κ_{xy}/T as a function of magnetic field H at fixed $T = 34.2$ K in the hole-doped cuprate $La_{2-x}Sr_xCuO_4$ $p = 0.06$ (LSCO). The red circles are obtained sweeping the magnetic field continuously at a rate of 0.7 T/min. The purple circles are obtained using a steady-state method as a function of field with steps of 1 T. The green square is obtained using a steady-state method as a function of temperature at $H = 15$ T.

FIG. 8. κ_{xy}/T as a function of temperature at $H = 15$ T in the hole-doped cuprate $La_{2-x}Sr_xCuO_4$ $p = 0.06$ (LSCO). The green squares are obtained using a steady-state method as a function of temperature. The purple circles are obtained using a steady-state method as a function of magnetic field.

(1) Steady-state method as function of temperature, also known as "T-steps" (see Figs. 7 and 8). The magnetic field H is kept fixed (at $+H$) while the temperature T of the sample is changed in discrete steps (2 to 3 K steps). At each temperature, the background voltage of the thermocouple that measures ΔT_y is recorded before the heat is applied to the sample. When the sample is in an equilibrium configuration, $\Delta T_y(H)$ is measured.

The background voltage of the thermocouple is carefully subtracted from the measured heat-on signal from the thermocouple. Once the entire temperature range is covered, say from 10 K to 100 K, the field direction is reversed to $-H$. The same procedure is followed for this field polarity. Then, the ΔT_y signal is antisymmetrized; $\Delta T_y(T, H) = [\Delta T_y(T, +H) - \Delta 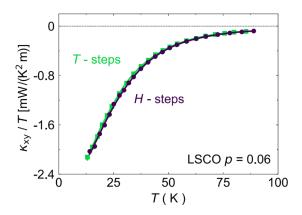T_y(T, -H)]/2$, such that any symmetric contribution, coming from the longitudinal thermal gradient due to misalignment of the transverse contacts, is removed.

(2) Steady-state method as a function of field, also known as "H-steps" (see Figs. 7 and 8). The temperature T is kept fixed, and the magnetic field H is changed in discrete steps (1 to 2 T steps). At a fixed temperature, a heat current $\vec{J}$ is sent to the sample, and once it reaches equilibrium, the magnetic field is changed from $+H$ to $-H$ in steps. For each field step h, we define $\Delta T_y(T, h) = [\Delta T_y(T, +h) - \Delta T_y(T, -h)]/2$. Once the entire magnetic-field range is covered, the temperature of the sample is changed and the same procedure is repeated.

(3) Field sweep method, also known as "H-sweeps" (see Fig. 7). This method is similar to (2), but now the magnetic field is continuously changed from $+H$ to $-H$.

We found satisfactory agreement between methods (1), (2), and (3), see Fig. 7.

[1] T. Ideue, T. Kurumaji, S. Ishiwata, and Y. Tokura, Giant thermal Hall effect in multiferroics, Nat. Mater. **16**, 797 (2017).

[2] G. Grissonnanche, A. Legros, S. Badoux, E. Lefrançois, V. Zatko, M. Lizaire, F. Laliberté, A. Gourgout, J.-S. Zhou, S. Pyon, T. Takayama, H. Takagi, S. Ono, N. Doiron-Leyraud, and L. Taillefer, Giant thermal Hall conductivity in the pseudogap phase of cuprate superconductors, Nature **571**, 376 (2019).

[3] G. Grissonnanche, S. Thériault, A. Gourgout, M.-E. Boulanger, E. Lefrançois, A. Ataei, F. Laliberté, M. Dion, J.-S. Zhou, S. Pyon, T. Takayama, H. Takagi, S. Ono, N. Doiron-Leyraud, and L. Taillefer, Chiral phonons in the pseudogap phase of cuprates, Nat. Phys. **16**, 1108 (2020).

[4] M.-E. Boulanger, G. Grissonnanche, S. Badoux, A. Allaire, E. Lefrançois, A. Legros, A. Gourgout, M. Dion, C. H. Wang, X. H. Chen, R. Liang, W. N. Hardy, D. A. Bonn, and L. Taillefer, Thermal Hall conductivity in the cuprate Mott insulators Nd_2CuO_4 and $Sr_2CuO_2Cl_2$, Nat. Commun. **11**, 5325 (2020).

[5] X. Li, B. Fauqué, Z. Zhu, and K. Behnia, Phonon thermal Hall effect in strontium titanate, Phys. Rev. Lett. **124**, 105901 (2020).

[6] L. Chen, M.-E. Boulanger, Z.-C. Wang, F. Tafti, and L. Taillefer, Large phonon thermal Hall conductivity in the antiferromagnetic insulator Cu_3TeO_6, Proc. Natl. Acad. Sci. **119**, e2208016119 (2022).

[7] C. Strohm, G. L. J. A. Rikken, and P. Wyder, Phenomenological evidence for the phonon Hall effect, Phys. Rev. Lett. **95**, 155901 (2005).

[8] M. Mori, A. Spencer-Smith, O. P. Sushkov, and S. Maekawa, Origin of the phonon Hall effect in rare-earth garnets, Phys. Rev. Lett. **113**, 265901 (2014).

[9] T. Qin, J. Zhou, and J. Shi, Berry curvature and the phonon Hall effect, Phys. Rev. B **86**, 104305 (2012).

[10] M. Ye, L. Savary, and L. Balents, Phonon Hall viscosity in magnetic insulators, arXiv:2103.04223.

[11] Y. Zhang, Y. Teng, R. Samajdar, S. Sachdev, and M. S. Scheurer, Phonon Hall viscosity from phonon-spinon interactions, Phys. Rev. B **104**, 035103 (2021).

[12] R. Samajdar, S. Chatterjee, S. Sachdev, and M. S. Scheurer, Thermal Hall effect in square-lattice spin liquids: A Schwinger boson mean-field study, Phys. Rev. B **99**, 165126 (2019).

[13] L. Mangeolle, L. Balents, and L. Savary, Phonon thermal Hall conductivity from scattering with collective fluctuations, Phys. Rev. X **12**, 041031 (2022).

[14] H. Guo and S. Sachdev, Extrinsic phonon thermal Hall transport from Hall viscosity, Phys. Rev. B **103**, 205115 (2021).

[15] B. Flebus *et al.*, Charged defects and phonon Hall effects in ionic crystals, Phys. Rev. B **105**, L220301 (2022).

[16] X.-Q. Sun, J.-Y. Chen, and S. A. Kivelson, Large extrinsic phonon thermal Hall effect from resonant scattering, Phys. Rev. B **106**, 144111 (2022).

[17] H. Guo, D. G. Joshi, and S. Sachdev, Resonant thermal Hall effect of phonons coupled to dynamical defects, Proc. Natl. Acad. Sci. **119**, e2215141119 (2022).

[18] M. Hirschberger, J. W. Krizan, R. J. Cava, and N. P. Ong, Large thermal Hall conductivity of neutral spin excitations in a frustrated quantum magnet, Science **348**, 106 (2015).

[19] Y. Hirokane, Y. Nii, Y. Tomioka, and Y. Onose, Phononic thermal Hall effect in diluted terbium oxides, Phys. Rev. B **99**, 134419 (2019).

[20] E. Lefrançois, G. Grissonnanche, J. Baglo, P. Lampen-Kelley, J.-Q. Yan, C. Balz, D. Mandrus, S. E. Nagler, S. Kim, Y.-J. Kim, N. Doiron-Leyraud, and L. Taillefer, Evidence of a phonon Hall effect in the Kitaev spin liquid candidate α-RuCl$_3$, Phys. Rev. X **12**, 021025 (2022).

[21] M.-E. Boulanger, G. Grissonnanche, E. Lefrançois, A. Gourgout, K.-J. Xu, Z.-X. Shen, R. L. Greene, and L. Taillefer, Thermal Hall conductivity of electron-doped cuprates, Phys. Rev. B **105**, 115101 (2022).

[22] A. Ataei, G. Grissonnanche, M.-E. Boulanger, L. Chen, E. Lefrançois, V. Brouet, and L. Taillefer, Phonon chirality from impurity scattering in the antiferromagnetic phase of Sr$_2$IrO$_4$, Nat. Phys. **20**, 585 (2024).

[23] Q. Meng, X. Li, L. Zhao, C. Dong, Z. Zhu, and K. Behnia, Thermal Hall effect driven by phonon-magnon hybridization in a honeycomb antiferromagnet, arXiv:2403.13306.

[24] X. Li, Y. Machida, A. Subedi, Z. Zhu, L. Li, and K. Behnia, The phonon thermal Hall angle in black phosphorus, Nat. Commun. **14**, 1027 (2023).

[25] I. Vinograd, K. R. Shirer, P. Massat, Z. Wang, T. Kissikov, D. Garcia, M. D. Bachmann, M. Horvati, I. R. Fisher, and N. J. Curro, Second order Zeeman interaction and ferroquadrupolar order in TmVO$_4$, npj Quantum Mater. **7**, 68 (2022).

[26] Z. Wang, I. Vinograd, Z. Mei, P. Menegasso, D. Garcia, P. Massat, I. R. Fisher, and N. J. Curro, Anisotropic nematic fluctuations above the ferroquadrupolar transition in TmVO$_4$, Phys. Rev. B **104**, 205137 (2021).

[27] P. Massat, J. Wen, J. M. Jiang, A. T. Hristov, Y. Liu, R. W. Smaha, R. S. Feigelson, Y. S. Lee, R. M. Fernandes, and I. R. Fisher, Field-tuned ferroquadrupolar quantum phase transition in the insulator TmVO$_4$, Proc. Natl. Acad. Sci. **119**, e2119942119 (2022).

[28] Y.-H. Nian, I. Vinograd, T. Green, C. Chaffey, P. Massat, R. R. P. Singh, M. P. Zic, I. R. Fisher, and N. J. Curro, Spin echo, fidelity, and the quantum critical fan in TmVO$_4$, Phys. Rev. Lett. **132**, 216502 (2024).

[29] M. P. Zic, M. S. Ikeda, P. Massat, P. M. Hollister, L. Ye, E. W. Rosenberg, J. A. W. Straquadine, Y. Li, B. J. Ramshaw, and I. R. Fisher, Giant elastocaloric effect at low temperatures in TmVO$_4$ and implications for cryogenic cooling, PNAS **121**, e2320052121 (2024).

[30] R. Feigelson, Flux growth of type RVO$_4$ rare-earth vanadate crystals, J. Am. Ceram. Soc. **51**, 538 (1968).

[31] S. H. Smith and B. M. Wanklyn, Flux growth of rare earth vanadates and phosphates, J. Cryst. Growth **21**, 23 (1974).

[32] H. Suzuki, T. Inoue, and T. Ohtsuka, Enhanced nuclear cooling and spin-lattice relaxation time in TmVO$_4$ and TmPO$_4$, Physica B+C **107**, 563 (1981).

[33] A. H. Cooke, S. J. Swithenby, and M. R. Wells, The properties of thulium vanadate – An example of molecular field behaviour, Solid State Commun. **10**, 265 (1972).

[34] G. Grissonnanche, F. Laliberté, S. Dufour-Beauséjour, M. Matusiak, S. Badoux, F. F. Tafti, B. Michon, A. Riopel, O. Cyr-Choinière, J. C. Baglo, B. J. Ramshaw, R. Liang, D. A. Bonn, W. N. Hardy, S. Krämer, D. LeBoeuf, D. Graf, N. Doiron-Leyraud, and L. Taillefer, Wiedemann-Franz law in the underdoped cuprate superconductor YBa$_2$Cu$_3$O$_y$, Phys. Rev. B **93**, 064513 (2016).

[35] B. Daudin and B. Salce, Thermal conductivity of rare earth vanadates and arsenates undergoing a cooperative Jahn-Teller effect, J. Phys. C **15**, 463 (1982).

[36] Q. J. Li, Z. Y. Zhao, C. Fan, F. B. Zhang, H. D. Zhou, X. Zhao, and X. F. Sun, Phonon-glass-like behavior of magnetic origin in single-crystal Tb$_2$Ti$_2$O$_7$, Phys. Rev. B **87**, 214408 (2013).

[37] W. Mutscheller and M. Wagner, Thermal conductivity of cooperative Jahn-Teller E-systems, Phys. Status Solidi B **134**, 39 (1986).

[38] W. Mutscheller and M. Wagner, The influence of magnetic fields on the thermal conductivity of the cooperative vibronic system TmVO$_4$, Phys. Status Solidi B **144**, 507 (1987).

[39] R. Hentrich, M. Roslova, A. Isaeva, T. Doert, W. Brenig, B. Büchner, and C. Hess, Large thermal Hall effect in α-RuCl$_3$: Evidence for heat transport by Kitaev-Heisenberg paramagnons, Phys. Rev. B **99**, 085136 (2019).